Optics and Lasers in Engineering 110 (2018) 244–252

Contents lists available at ScienceDirect

Optics and Lasers in Engineering

journal homepage: www.elsevier.com/locate/optlaseng

Full-field deformation and temperature measurement for CW laser irradiated structures

Wu Yuan[a,b], Jiangtao Wang[a,b], Hongwei Song[a,b,*], Chenguang Huang[a,b]

[a] Key Laboratory for Mechanics in Fluid-Solid Coupling Systems, Institute of Mechanics, Chinese Academy of Sciences, Beijing 100190, China
[b] School of Engineering Sciences, University of Chinese Academy of Sciences, Beijing 100049, China

ARTICLE INFO

Keywords:
Full-field deformation
CW laser
Digital image correlation
Ablation

ABSTRACT

This paper presented a three dimensional deformation and full-field temperature measurement method for continuous wave laser irradiated structures over a range extending from the room temperature to the melting point. The deformation was measured by the three dimensional digital image correlation technique. The speckle pattern was made on the specimen surface by the high temperature glue with a maximum service temperature of 1700 ˚C. A bandpass filter and a blue light source were used to eliminate the effect of thermal radiation from the laser irradiated region. The accuracy of present method was validated by the coordinate measurement machine and the laser Doppler vibrometer. According to the relationship between the gray value of images and the temperature, the full-field temperature distribution were measured by the colorimetry temperature measurement method. Finally, parameters that affect the response of laser irradiated thin plates, including laser power, high-speed airflow, plate thickness and material properties are investigated.

1. Introduction

When exposed to continous wave (CW) laser irradiation, the absorbed laser energy by the material surface transforms into the internal heat energy of the target. Then, non-uniform temperature distribution is formed by the conduction of the heat energy from the irradiated region. Previous studies showed that the CW laser induced temperature damaged the target in different forms, according to the laser powers.

The mass loss is one of the main failure mode for the high-power laser irradiated structures, including melt, evaporation, pyrolysis and oxidation of the material [1]. When the laser power decreased, high temperature rise may cause the reduction of the elastic modulus, yield stress, fracture stress and, consequently, the strength of the target [2]. For thin-walled structures, thermal deformation induced by the development of compressive thermal stresses when temperatures of the laser irradiated zone below those that impair the material properties will also reduce the load bearing capability [3]. In addition, the outside environment may also affect the damage threshold of the irradiated structures. The presence of the tangential airflow will enhance the rate of the material removal and the melt-through time, even though the temperature of the target is under the melting point of the material [4]. The airflow may also dissipate part of input energy through convective cooling when the laser intensity varies [5]. Except for the laser induced damage threshold, the thermal deformation of the irradiated target is also strongly affected by the laser power, airflow, geometric and material parameters. However, the measurement of three dimensional (3D) deformation of structures at high temperature is still a challenging problem.

Some contact techniques which are conventionally used in the room temperature, such as displacement sensors, may be invalid in high temperature environments. The high-temperature strain gauge is insufficient to capture the full-field response of the structure and large-scale experiments are not easily carried out due to the high cost of this measurement method. In addition, there are a variety of non-contact optical methods have been proposed for surface deformation measurements of high temperature objects [6–10]. These methods mainly include interferometric techniques, such as strain/displacement gauge and moiré interferometry, and non-interferometric techniques, such as three dimensional digital image correlation (3D-DIC). Wang et al. [11] also proposed the mark shearing method to the thermal deformation of the high-temperature metal alloy at 1000 ˚C. Although the interferometric for high temperature deformation measurements are able to provide three dimensional deformation of structures, they do have inherent limitations such as low resolution [12].

Peters and Ranson [13] proposed the digital image correlation technique in 1981 by using the computer-based analysis for planar deformation measurements, which is simplified as 2D-DIC. However, 2D-DIC technique is limited to planar specimens that experience no out-of-plane motion. Luo et al. solved this problem by use of two digital cameras ob-

* Corresponding author at: Institute of Mechanics, Chinese Academy of Sciences, No.15 Beisihuanxi Road, Beijing 100190, China.
E-mail address: songhw@imech.ac.cn (H. Song).

https://doi.org/10.1016/j.optlaseng.2018.04.023
Received 19 December 2017; Received in revised form 21 March 2018; Accepted 29 April 2018
Available online 28 June 2018

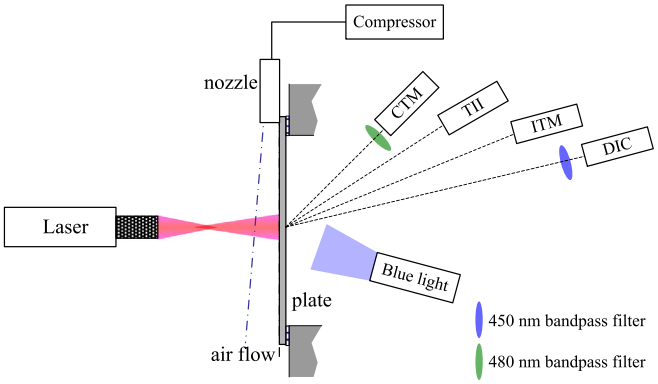

Fig. 1. Schematic of the experimental setup.

serving the surface from two different directions [14]. The 3D-DIC technique have been widely used for the measurement of displacements or strains in different fields [15–19]. In the high temperature environment, Wu et al. [20,21] measured the thermal linear expansion of the ceramic plate and the high temperature failure behaviour thermal barrier coating by using the 3D-DIC system. However, when being used in the high temperature environment, the measurement is restricted by the optical obstacle, and there are a number of issues that have to be considered in order to measure the deformation accuratly and robustly [22]:

(a) Most common coating material will burn or peel off during the test, changing the speckle shape.
(b) Black-body radiation, the light from the surface of heated samples or the heating system, alters the contrast of the images collected by the cameras.
(c) Heat haze, which results from the heating system, can cause local changes in the refractive index, distorting the view of the object.

This paper gives the full-field temperature and displacement measurement for the laser irradiated structures from room temperature to the melting point. Thermal deformation and temperature are mainly measured by the 3D-DIC technique and colorimetry temperature measurement method (CTM) respectively. The high temperature speckle was made on the specimen surface by using the high temperature glue. The bandpass filter and blue light source were used to eleminate the effect of the thermal radiation. The precision of the present measurement technique is validated by comparing the 3D deformation of the thin plate measured from the present technique with that from the contact measure technique coordinate measure machine (CMM) and the laser Doppler vibrometer (LDV). The accuracy of the CTM is validated by comparison of the spot center temperature on the back-surface measured by the CTM with that from the infrared thermometer (ITM) . The effect of laser power, material properties, geometric parameters and high-speed airflow on the deformation and temperature of thin plates are investigated.

2. Experimental procedure

2.1. Experimental setup

Fig. 1 shows the schematic of the experimental setup. A fiber laser with a maximum power of 2 kW operating at 1.07 μm and a CO_2 laser with a maximum power of 200 W operating at 1064 μm were used to irradiate the thin plates. Three types of samples were considered: aluminium plates with 0.5 mm thickness, SUS304 stainless steel plate with thickness of 0.9–2.7 mm, and GH625 high-temperature alloy plate with thickness of 2.0 mm. The LC4 aluminium plate was irradiated by the CO_2 laser with power of 50–200 W and the SUS304 stainless steel and GH625 high temperature alloy plates were irradiated by the fiber laser with the power of 500–2000 W.

A nozzle was placed at one side of the plate to deliver uniform airflow on the laser irradiated surface. The temperature of the airflow is −103 ˚C, and the speed is Mach 2. The deformation was measured by the 3D-DIC, which composed of two CCD cameras in two different directions. The full-field temperature distribution was measured by the CTM, thermal infrared imager (TII), and the ITM respectively. The temperature is measured by the TII for aluminium plates with low temperatures and the high-power laser irradiated stainless steel and high-temperature alloy plate are measured by the CTM.

2.2. Measurement of 3D deformation

Several special steps are needed to obtain the 3D deformation of laser irradiated thin plates, due to the high temperature effect. For the 3D-DIC technique, the specimen surface must be coated with some random speckle patterns with appropriately sizes. The speckle used in high temperature must satisfy the following requirements [23].

(a) The speckle must maintain its color and hold the shape during the heating process. Unexpected change in the shape may adversely affect the result of the image correlation.
(b) The speckle must adhere to the surface of the specimen stably and deform simultaneously with the specimen's surface without cracking and peeling off.

To measure the 3D deformation evolution of the high-power laser irradiated stainless steel plate, which has a melting point of about 1400 ˚C, the specimen was sprayed with a thin layer of white inorganic glue that can withstand temperature of 1730 ˚C. Then, the high temperature black paint was sprayed on the surface of the inorganic glue to make the high temperature speckle. During the experiment, the light from the thermal radiation of the high temperature region saturates the speckle image brightness and decreases the image contrast dramatically. Then, a serious decorrelation effect occurs among the images to be matched. In addition, there is a significant temperature gradient in the specimen, and the specimen also experience a significant temperature change during laser irradiation. Therefore, as shown in Fig. 2(a), the speckle image cannot be captured clearly over the whole region of the specimen and the whole process of laser irradiation by simply decreasing the illumination of the CCD camera.

As the temperature rises, although the total amount of thermal radiation increases dramatically, the absolute intensity change induced by thermal radiation at short wavelength (e.g., 450 nm) is negligible [24]. Therefore, a bandpass optical filter and a blue illumination light source with associated wavelength were used to eliminate the effect of thermal irradiation. Fig. 2(b) shows the speckle images of 500 W fiber laser-irradiated stainless-steel plate with 0.9 mm thickness measured by the CCD camera with the blue light and the bandpass filter. The failure process of the speckle on the surface of the stainless specimen can be clearly captured by using the present method. So, the present method is more suitable to the measurement of full-field deformation for structures with high non-uniform temperature distribution.

The gray value correlation function used in this paper is the normalized covariance correlation function, which can be written as

$$C(u,v)=\frac{\sum_{x'=0}^{m-1}\sum_{y'=0}^{n-1}\left[I_0(x,y)-\bar{I}_0\right]\left[I(x'+x,y'+y)-\bar{I}\right]}{\sqrt{\sum_{x'=0}^{m-1}\sum_{y'=0}^{n-1}\left[I_0(x,y)-\bar{I}_0\right]^2}\sqrt{\sum_{x=0}^{m-1}\sum_{y=0}^{n-1}\left[I(x'+x,y'+y)-\bar{I}\right]^2}} \tag{1}$$

Where x and y are the coordinates of the original image, and x' and y' are the coordinates of the target image. x_0 and y_0 are the coordinates of the template center. u and v are displacements at x and y directions. m and n are the size of the compute template, $I_0(x, y)$ is the gray value of the point (x, y) on the source image and $I(x', y')$ is the gray value of the point (x', y') on the target image. $\bar{I}_0$ and $\bar{I}$ are the average gray value of compute template on the source and target image respectively.

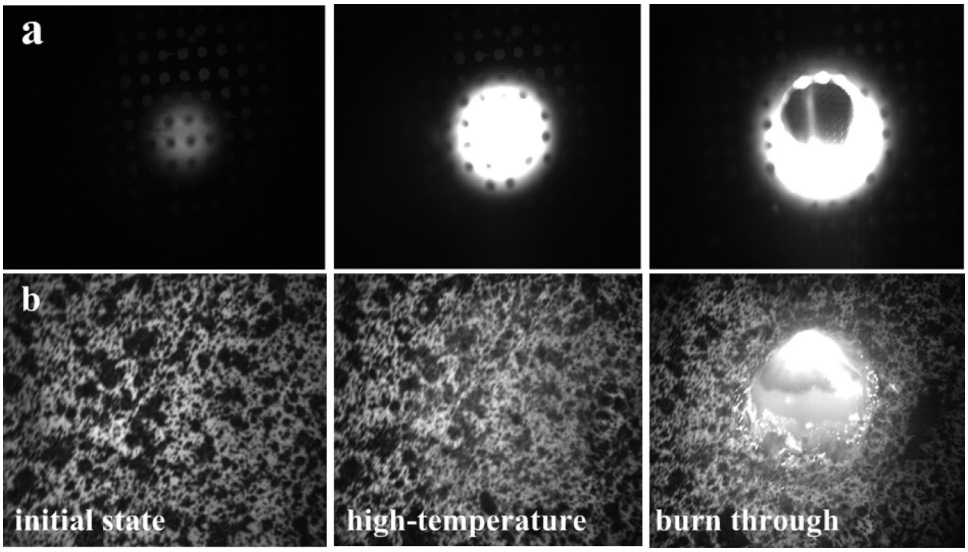

Fig. 2. Speckle images acquired in the present experiment. (a) without filters and the irradiation of the blue light (b) with filters and the irradiation of the blue light and filters.

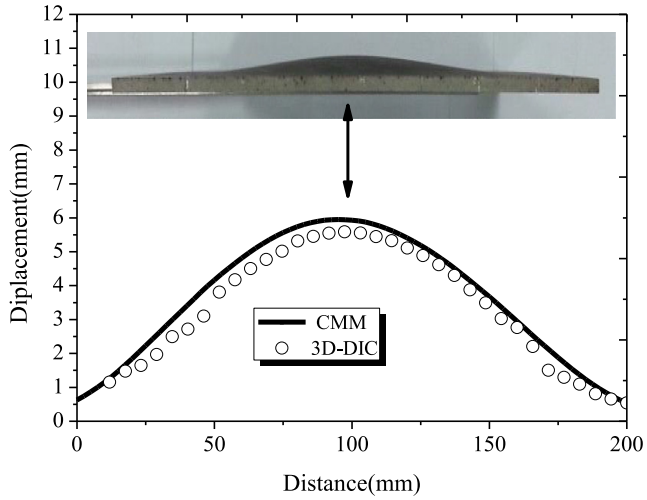

Fig. 3. Comparison of measured deformation profile between 3D-DIC technique and CMM.

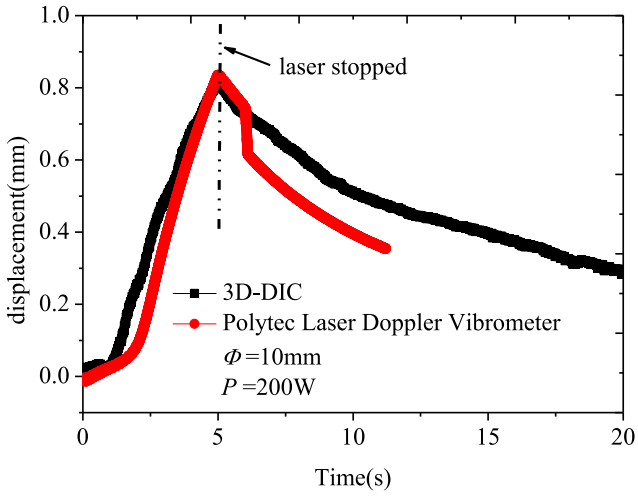

Fig. 4. Comparison of the maximum out-of-plane deformation measured from 3D-DIC technique and LDV.

To maximize the correlation coefficient, one yields

$$\frac{\partial C}{\partial p_i} = 0, i = 1, 2, \ldots 12 \tag{2}$$

The sub-pixel iterative algorithm Newton–Rapson method is used as the correlation function

$$P^{k+1} = P^k + \Delta P \tag{3}$$

$$\Delta P = -H^{-1} \nabla P \tag{4}$$

where H is the hessian matrix, and ∇P is the Jacobi vector. P^k and P^{k+1} are the value of the unknown parameters of the shape function at the k and $k+1$ iteration.

As shown in Fig. 3, the precision of present deformation measurement method can be validated by comparison of the out-of-plane deformation of a deformed aluminum plate measured from the present 3D-DIC technique with that from the contact measurement technique CMM, which has a precision of 2 μm. The deformation process of the specimen was also compared with that measured from the LDV with a resolution of 1 nm, as shown in Fig. 4. Both the deformation mode and the deformation process are in a agreement with that from the CMM and the LDV.

2.3. Measurement of full-field temperature

For the moment, the high temperature field also can be measured by the well-established IR camera [25]. However, IR camera is easily affected by the smoke, dust, stream and the emission ration of materials. In contrast, the CTM is not sensitive to environmental interference. More importantly, optical glass is always used to protect the target environment, for example, in a vacuum environment or in the wind tunnel. However, the working waveband of general IR cameras (3 μm-5 μm or 8 μm-14 μm) is not in the transparent range of most heat-resistant optical glasses (below 3 μm). In this condition, the IR camera is inapplicable and the CTM is imperative.

For thin-walled structures, the back-surface temperature is raised to the melting point in a short time. The spectral radiance emitted from the high temperature region can be obtained based on Planck's law and

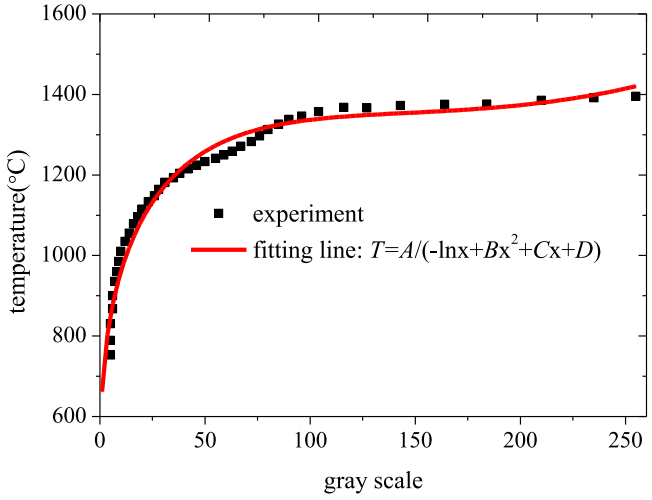

Fig. 5. The relation between the gray scale of the captured image and the temperature.

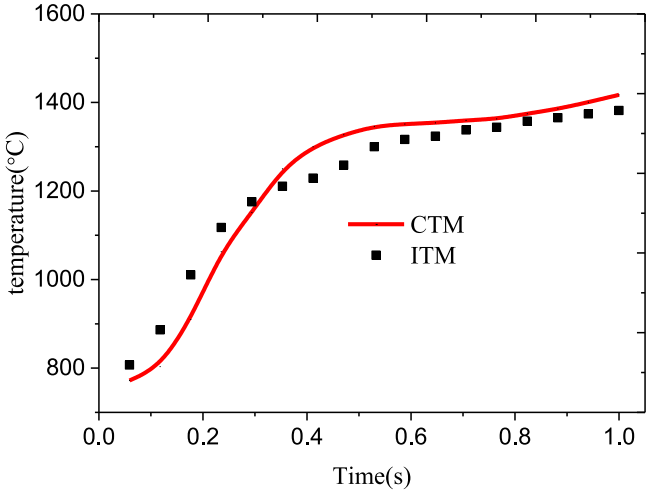

Fig. 6. Comparison of the spot-center temperature on the back-surface measured from the CTM with that from the ITM.

Wien's law [26]

$$M(\lambda,T)=C_1\varepsilon(\lambda,T)\lambda^{-5}\exp\left(-\frac{C_2}{\lambda T}\right) \tag{5}$$

where λ is the wavelength (less than 800 μm in this equation). C_1 and C_2 are the first radiance constant and second radiation constant. T is the temperature.

The spectral radiant flux Φ from the interaction zone to the detector is [27]

$$\Phi_\lambda=\int_A \varepsilon(\lambda,T)M(\lambda,T)\cos\theta\Omega dA \tag{6}$$

where ε, θ are emission ratio and emission angle of the specimen to be measured. Ω and A are the solid angle and area of measured spot respectively.

Supposing the object is at the temperature T, spectral radiance of two different wavelength λ_1, λ_2 are $M(\lambda_1, T)$, $M(\lambda_2, T)$.

$$\ln\frac{M(\lambda_1,T)}{M(\lambda_1,T)}=\ln\frac{\varepsilon(\lambda_1,T)}{\varepsilon(\lambda_1,T)}-5\ln\frac{\lambda_1}{\lambda_2}+\left(\frac{1}{\lambda_1}-\frac{1}{\lambda_2}\right)\frac{C_2}{T} \tag{7}$$

$\varepsilon(\lambda_1, T)$ and $\varepsilon(\lambda_1, T)$ are the emission ratios of λ_1 and λ_2 respectively.

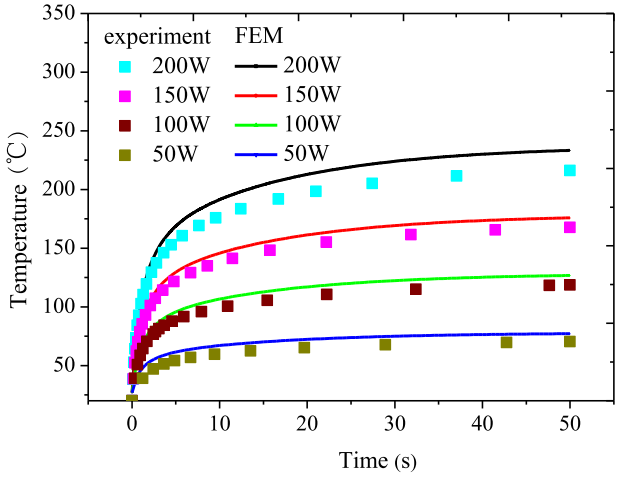

Fig. 7. Temperature histories of spot center of aluminum plates irradiated by CW laser with different powers.

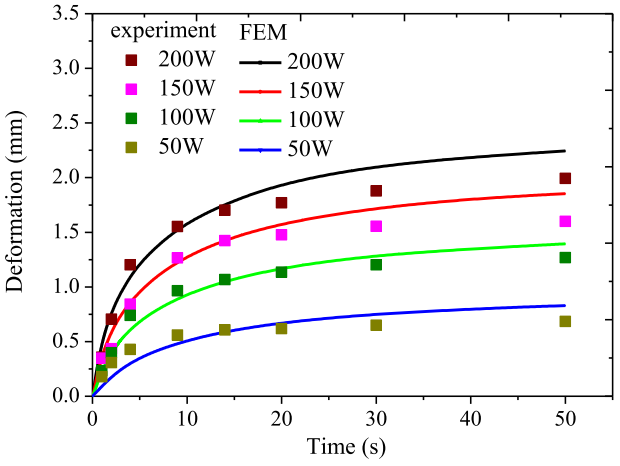

Fig. 8. Comparison of thermal deformation of aluminum plates measured from the 3D-DIC technique with that from the FEM.

When the wavelengths of λ_1 and λ_2 are close to each other, the variation of emission ratios of the two lights with the increasing temperature are basically the same. Therefore, the emission ratios can be considered equal, and the effects of emission ratio in the first item of Eq. 7 $\ln\frac{\varepsilon(\lambda_1,T)}{\lambda_1,T}$ can be removed.

The energy absorbed by the CCD camera is integration of the spectral radiant flux and the spectral sensitivity over the whole spectral range

$$S=\int_0^\infty R_\lambda(\lambda)M(\lambda,T)d\lambda \tag{8}$$

where S, R_λ are detector signal and spectral sensibility of the optical system.

The back-surface temperature of the specimen can be measured according to the gray value in images collected by the CCD camera in a specific wavelength, which have a relationship with the target temperature. By fitting gray values of a series of images collected by CCD and temperature measured by ITM, the relationship is obtained as the following form, as shown in Fig. 5.

$$T=\frac{A}{-\ln x+Bx^2+Cx+D} \tag{9}$$

The CCD camera of Prosilica GT4905 with a sampling rate of 17 Hz is used to collect the gray value image of the back-surface of the stainless-steel specimen. The distance between the camera and the specimen is

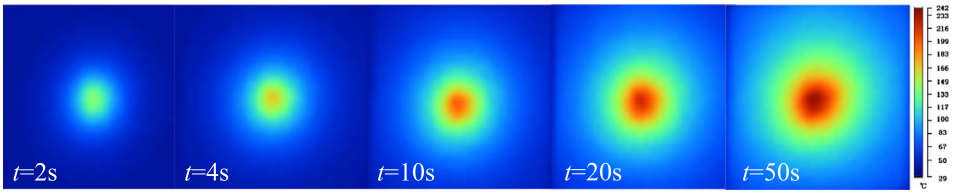

Fig. 9. Full-field temperature distribution of aluminum plate measured by the TII with laser power $P = 200$ W, spot diameter $\phi = 15$ mm.

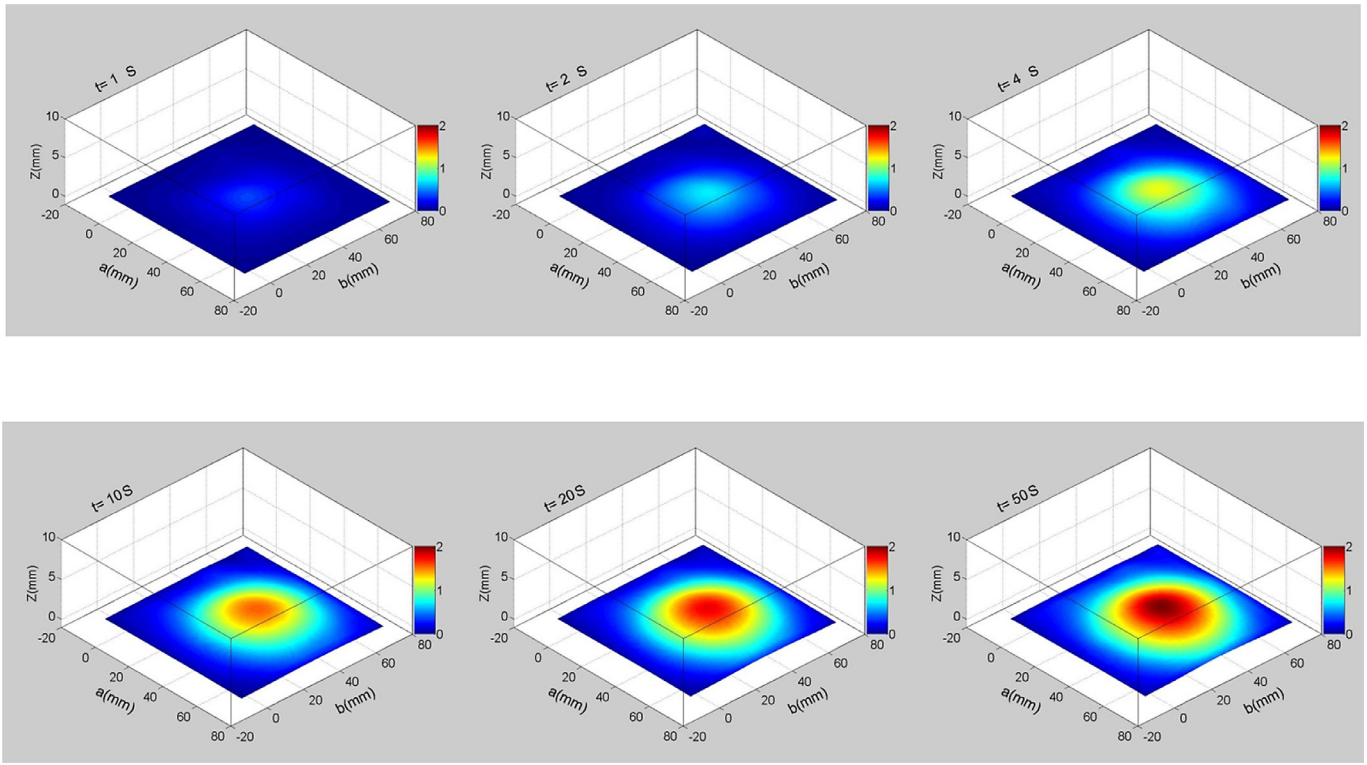

Fig. 10. Thermal deformation of aluminum plate measured by the 3D-DIC technique with laser power $P = 200$ W, spot diameter $\phi = 15$ mm.

about 1300 mm and the angle is 30°. A 480 nm band-pass filter with the bandwidth of 25 nm and a 10% neutral attenuation slice are set in front of the camera to get the distribution of the gray value evolutions of the back-surface. As shown in Fig. 6, the accuracy of the present temperature measurement method can be validated by the comparison of the spot-center temperature on the back-surface measured from the CTM with that from the ITM, which has a measurement error 0.75%.

3. Experimental results

3.1. Low-power CW laser experiment

The low-power irradiated aluminum plate will reach a thermal equilibrium state in a few seconds due to the thermal convection and thermal radiation of the high-temperature zone. Thermal deformation induced by thermal stresses during the laser irradiation process is the main failure mode. The spot diameter of the laser is 15 mm, and the laser power P ranges from 50 W to 200 W. The size and the thickness of the aluminum plate are 80×80 mm^2 and 0.5 mm respectively. The temperature distribution of the back-surface is measured by the TII Fluke Ti55. The resolution is 320×240 pixel. The temperature range selected in the present paper is −20~350 °C. The accuracy of the TII is ± 2 °C.

3.1.1. In natural convection environment

Thermal-structural responses of the laser irradiated aluminum plate were also simulated by a series of finite element models (FEM), based on the commercial software ABAQUS. Figs. 7 and 8 shows the comparison of temperature histories of the spot center obtained from the TIC and FEM, when the laser power is raised from 50 W to 200 W. The experimental results are in a good agreement with those of FEM. The maximum temperature rise and thermal deformation of the aluminum plates increase with the laser power.

Fig. 9 shows the measured full-field temperature distribution of the back-surface of the aluminum plate at different times when the laser power is 200 W. The temperature rise of the plate grows rapidly upon laser irradiation, and the maximum temperature of 242 °C is reached at about 50 s. As shown in Fig. 10, the symmetric thermal deformation of the thin aluminum plate is increased with the irradiation time. The maximum deformation is about 2 mm when the irradiation time is 50 s. Fig. 11 shows the full-field temperature distribution and 3D deformation of the thin plate irradiated by the laser with different powers when the irradiation time is 50 s.

3.1.2. In high-speed airflow environment

To study the effect of the high-speed airflow, a nozzle with an exit velocity of Mach 2 is designed. The laser power in this experiment is 200 W. Fig. 12 shows the measured temperature history of the point with a distance of 20 mm from the spot center of the aluminum plate.

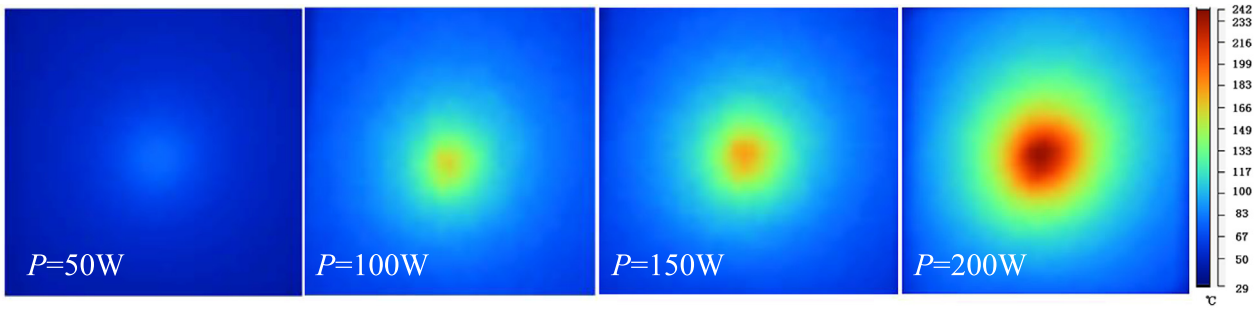

(a) Full-field temperature distribution

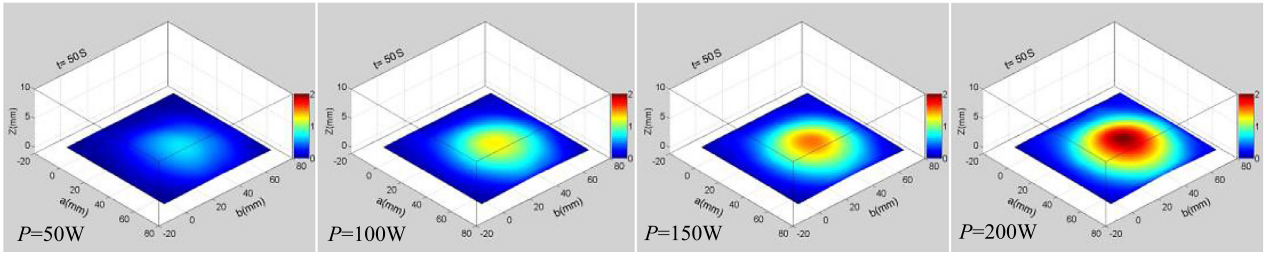

(b) 3D thermal deformation

Fig. 11. 3D deformation and temperature distribution of thin plate subjected to various laser power, from 50 W to 200 W with laser spot of $\phi = 15$ mm, after 50 seconds irradiation.

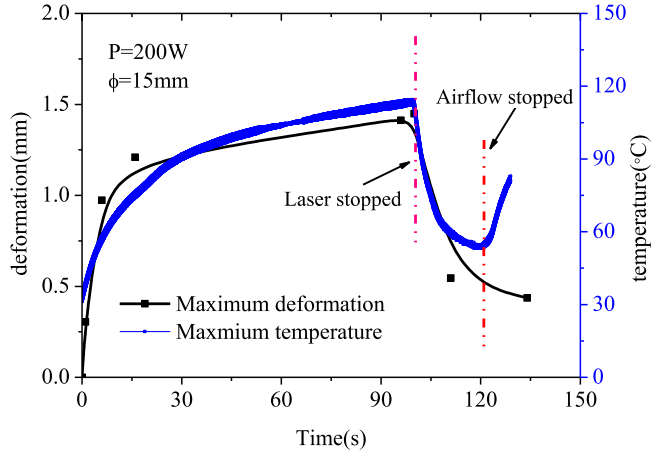

Fig. 12. Thermal deformation and temperature histories of thin aluminum plate in high-speed airflow.

The evolution of the temperature rise is similar to the temperature rise without the airflow. However, the presence of the cooling airflow reduce the temperature of the aluminum plate. As a result, the deformation of the aluminum plate exposed to the high-speed airflow is smaller than that without the airflow. When the CW laser stopped at 100 s, the thermal deformation decreases dramatically due to the cooling effect of the high-speed airflow.

Except for the cooling effect, the high-speed airflow also changes the temperature distribution and the deformation mode of the aluminum plate, as shown in Fig. 13. The comparison of the deformation mode of the aluminum plate without and with the high-speed airflow is shown in Fig. 14. Due to the effect of the airflow, the temperature distribution of the plate is transformed from the circle to ellipse mode, and correspondingly, the deformation mode also experiences this kind of transformation.

3.2. High-power CW laser experiment

In this section, the fiber laser with power of 500–2000 W was used to irradiate the stainless and high-temperature alloy plate. The diameter of the laser spot is 10 mm, which is obtained by adjusting the distance from the laser head to the plate. Ablation of the irradiated zone due to the solid-liquid phase change at high temperature is the main failure mode of the high-power CW laser irradiated metallic specimen. Before the temperature reaching the melting point, the thermal deformation induced by the non-uniform temperature distribution is also developed for the thin plate. The evolution of full-field temperature during the laser irradiation process is measured by the CTM.

Fig. 15 shows the 3D deformation of the 500 W CW laser irradiated SUS304 stainless steel plate with 0.9 mm thickness. It can be found that the deformation of the thin plate can be measured even when the temperature reaches the melting point. The thermal deformation is increased with an increase in the irradiation time. Then, the metallic solution erupted from the laser irradiated zone, and the speckle pattern on the specimen surface was destroyed. The full-field temperature of the back-surface was measured by the CTM, as shown in Fig. 16.

The stainless-steel plate with 2.7 mm thickness and GH625 high-temperature alloy plate with 2 mm thickness are also irradiated by 2000 W laser to study the effect of plate thickness and material properties. Fig. 17 compares of the out-of-plane deformation of back-surface for plates with different thickness and materials. The flexural stiffness of the thin plate is significantly increased with an increase in thickness. Therefore, the thermal deformation of the plate with smaller thickness is more obvious. Besides, the material properties, especially the thermal expansion coefficient, also affect the deformation of the thin plate dramatically. The deformation of GH625 high-temperature alloy plate, which has a thermal expand coefficient of $1.2 \times 10^{-5}/°C$, is smaller than that with SUS304 stainless steel plate, which has a thermal expand coefficient of $1.7 \times 10^{-5}/°C$.

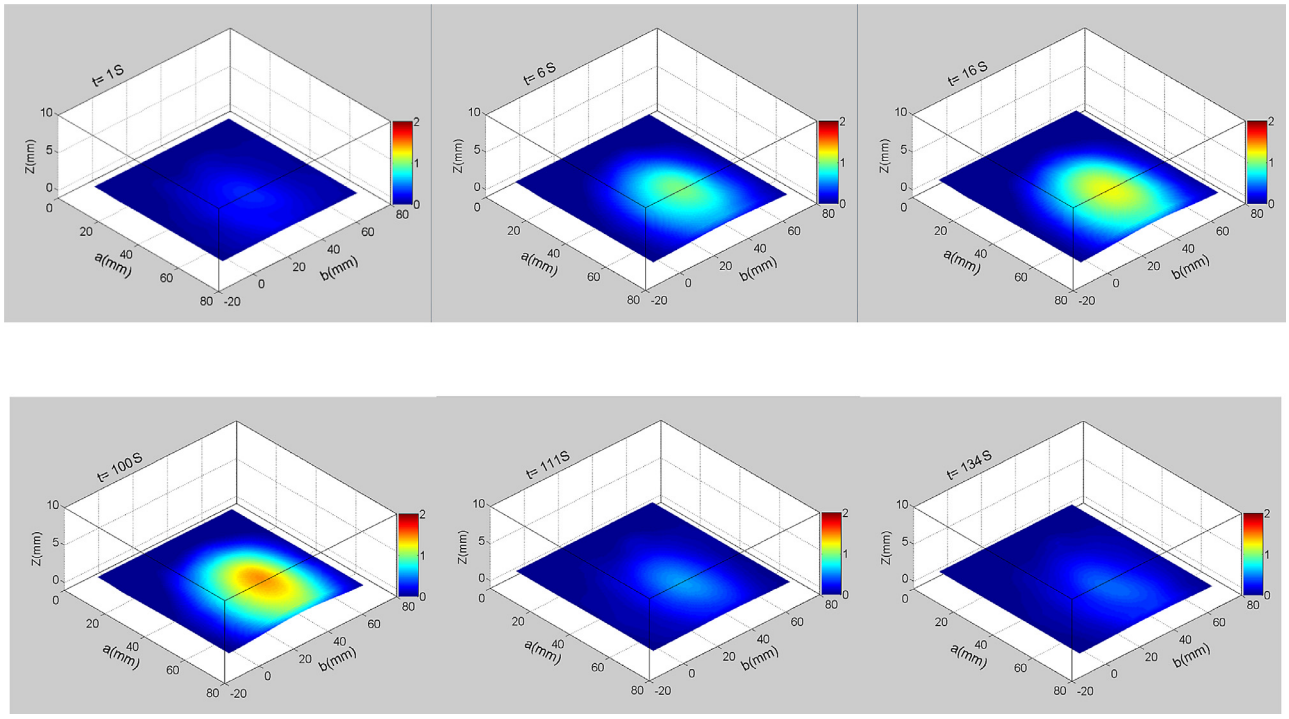

Fig. 13. Deformation mode of aluminum plate in high-speed airflow environment with laser power $P = 200$ W, spot diameter $\phi = 15$ mm.

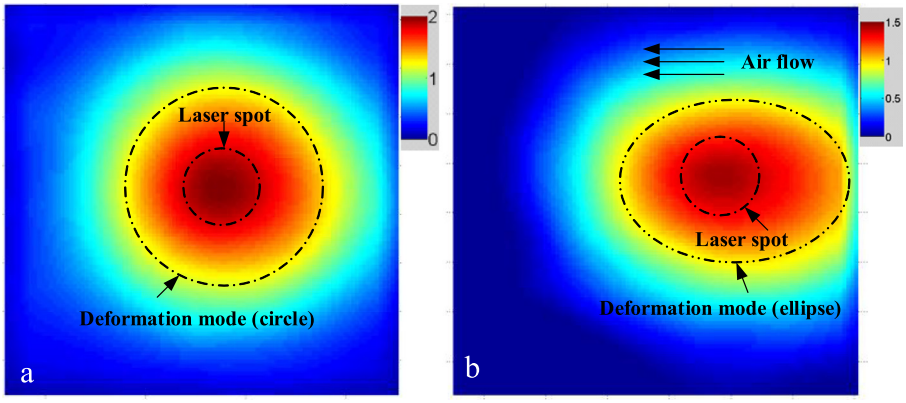

Fig. 14. Comparison of deformation modes of aluminum plates without airflow and with airflow. (a) without airflow, (b) with airflow.

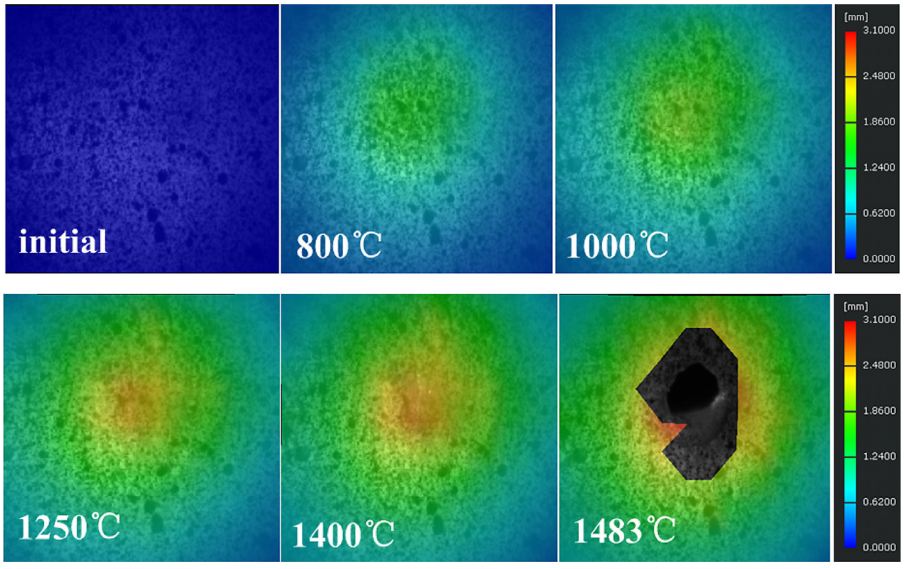

Fig. 15. 3D deformation of stainless steel plates measured by the 3D-DIC.

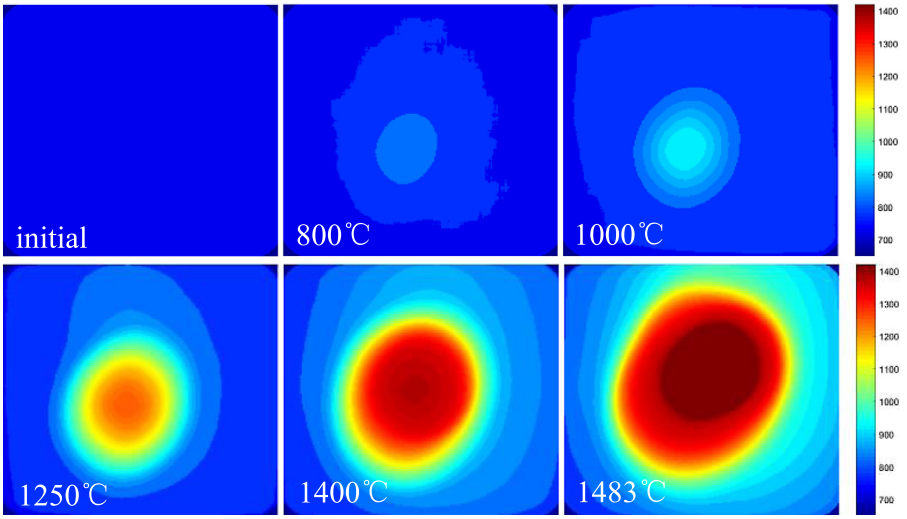

Fig. 16. Full-field temperature distribution of stainless steel plates measured by the CTM.

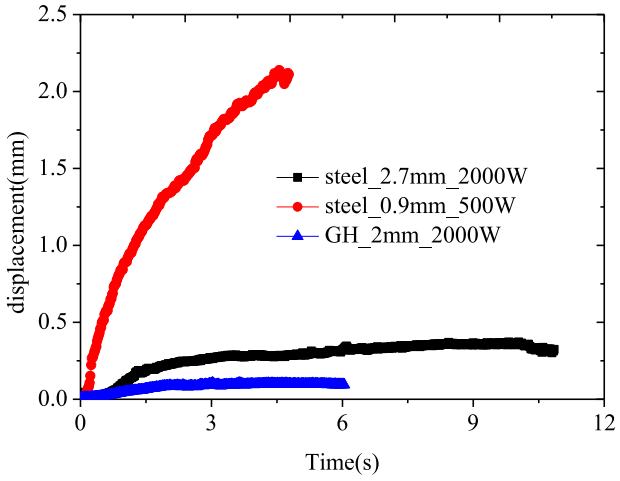

Fig. 17. Comparison of the maximum out-of-plane deformation of thin plates with different plate thickness and material properties.

4. Conclusions

This paper presents a method to measure the full-field temperature and 3D deformation for thin-walled structures irradiated by CW laser. The evolution of the deformation was obtained from room temperature to the temperature reaches the melting point. The full-field temperature was measured by the CTM and the TII respectively. The precision of the 3D-DIC technique was validated by the CMM and the LDV. By using the present measurement method, series of experiments are carried out, and effects of laser power, plate thickness, material properties and high-speed airflow on the thermal-structural response of thin plates irradiated by CW laser are discussed. Experimental results show that the presence of the high-speed airflow changes the temperature mode and deformation mode of the plate from circle mode to ellipse mode. When the laser power is increased, the ablation of the laser irradiated zone is the main failure mode. The plate thickness and material properties also affect the thermal deformation of thin plates dramatically.

Acknowledgments

Financial supports from National Natural Science Foundation of China (grant nos. 91016025, 11472276, 11602271, 11332011 and Defense Industrial Technology Development Program of China, No. JCKY2016130B009) are gratefully acknowledged.

References

[1] Volkov AN, Zhigilei LV. Melt dynamics and melt-through time in continuous wave laser heating of metal films: Contributions of the recoil vapor pressure and Marangoni effects. Int J Heat Mass Transf 2017;112:300–17.
[2] Jelani M, Li ZW, Shen ZH, Sardar M. Failure response of simultaneously pre-stressed and laser irradiated aluminum alloys. Appl Sci-Basel 2017:7.
[3] Chen Y, Li S. Buckling failure of the axially pre-compressed cylindrical shell irradiated by CW CO2 laser beam. 24th Plasma Dynamics, and Lasers Conference. American Institute of Aeronautics and Astronautics; 1993.
[4] Boley CD, Cutter KP, Fochs SN, Pax PH, Rotter MD, Rubenchik AM, Yamamoto RM. Interaction of a high-power laser beam with metal sheets. J Appl Phys 2010:107.
[5] Baek WK, Lee KC, An SI, Shin WS, Yoh JJ. Melt-through characteristics in continuous beam irradiation of flying metal samples in flow speeds up to 85m/s. Opt Laser Technol 2013;45:250–5.
[6] Anwander M, Zagar BG, Weiss B, Weiss H. Noncontacting strain measurements at high temperatures by the digital laser speckle technique. Exp Mech 2000;40:98–105.
[7] Løkberg OJ, Malmo JT, Slettemoen GÅ. Interferometric measurements of high temperature objects by electronic speckle pattern interferometry. Appl Opt 1985;24:3167–72.
[8] Post D, Wood J. Determination of thermal strains by moiré interferometry. Exp Mech 1989;29:318–22.
[9] Sharpe W Jr. A high-frequency high-temperature optical strain/displacement gage. Exp Mech 2010;50:227–37.
[10] Völkl R, Fischer B. Mechanical testing of ultra-high temperature alloys. Exp Mech 2004;44:121–7.
[11] Wang HX, Xie HM, Dai XL, Wu LF. Study on the high temperature deformation measurement using the mark shearing technique. Meas Sci Technol 2015:26.
[12] Pan B, Wu D, Wang Z, Xia Y. High-temperature digital image correlation method for full-field deformation measurement at 1200 C. Meas Sci Technol 2011;22:015701.
[13] Peters WH, Ranson WF. Digital imaging techniques in experimental stress-analysis. Opt Eng 1982;21:427–31.
[14] Luo P, Chao Y, Sutton M, Peters W III. Accurate measurement of three-dimensional deformations in deformable and rigid bodies using computer vision. Exp Mech 1993;33:123–32.
[15] Li J-Y, Lau A, Fok AS. Application of digital image correlation to full-field measurement of shrinkage strain of dental composites. J Zhejiang Univ Sci A 2013;14:1–10.
[16] Li L, Gong M, Chui Y, Schneider M, Li D. Measurement of the elastic parameters of densified balsam fir wood in the radial-tangential plane using a digital image correlation (DIC) method. J Mater Sci 2013;48:7728–35.
[17] Machado G, Favier D, Chagnon G. Membrane curvatures and stress-strain full fields of axisymmetric bulge tests from 3D-DIC measurements. Theory and validation on virtual and experimental results. Exp Mech 2012;52:865–80.
[18] Raurova I, Berggreen C, Eriksen R. A dual 3D DIC-system application for DSL strain and displacement measurements. In: EPJ Web of Conferences. EDP Sci; 2010. p. 31005.
[19] Wentzell S, Sterling Nesbitt R, Macione J, Kotha S. Measuring strain using digital image correlation of second harmonic generation images. J Biomech 2013;46:2032–8.
[20] Wu LF, Shi WX, Xie HM. Experimental study of high temperature failure behavior of thermal barrier coating based on 3D digital image correlation of single camera. J Exp Mech 2017.

[21] Wu LF, Zhu JG, Xie HM. Single-lens 3D digital image correlation system based on a bilateral telecentric lens and a bi-prism: validation and application. Appl Opt 2015;54:7842–50.
[22] Grant B, Stone H, Withers P, Preuss M. High-temperature strain field measurement using digital image correlation. J Strain Anal Eng Des 2009;44:263–71.
[23] Chen X, Xu N, Yang LX, Xiang D. High temperature displacement and strain measurement using a monochromatic light illuminated stereo digital image correlation system. Meas Sci Technol 2012;23:1–9.
[24] Pan B, Wu DF, Wang ZY, Xia Y. High-temperature digital image correlation method for full-field deformation measurement at 1200 °C. Meas Sci Technol 2011:22.
[25] The VIC-3D IR System-Technology Overview.
[26] G.B. Rybicki, A.P. Lightman, Radiative processes in astrophysics, Wiley 1979.
[27] Bi GJ, Gasser A, Wissenbach K, Drenker A, Poprawe R. Identification and qualification of temperature signal for monitoring and control in laser cladding. Opt Laser Eng 2006;44:1348–59.